GREENHOUSE GASES SCIENCE AND TECHNOLOGY

Effects of variable injection rate on reservoir responses and implications for CO_2 storage in saline aquifers

Cai Li and Federico Maggi, School of Civil Engineering, The University of Sydney, NSW, Australia
Keni Zhang, Institute of Groundwater and Earth Sciences, Jinan University, Guangzhou, China
Chaobin Guo, Chinese Academy of Geological Sciences, Beijing, China
Yixiang Gan and Abbas El-Zein, School of Civil Engineering, The University of Sydney, NSW, Australia
Zhejun Pan, CSIRO Energy Business Unit, Clayton South, Victoria, Australia
Luming Shen, School of Civil Engineering, The University of Sydney, NSW, Australia

Abstract: Past reservoir simulations of carbon dioxide (CO_2) storage in saline aquifers have shown that the injection procedure can influence CO_2 storage efficiency and injectivity. To investigate the influence of injection rate and timing on reservoir dynamics and storage performance, scenarios of continuous and intermittent injections were devised for storing 1 million tonnes of CO_2 per year for 30 years and were assessed through numerical simulations on saline aquifers constructed with real field data. Our results show that almost all the intermittent injections need higher injection pressure than the constant injection for the same targeted amount of CO_2. Only one intermittent injection showed the potential to have a lower injection pressure than the constant injection. The injectivity for the constant injection consistently declines over the years, while the intermittent injections result in an injectivity above a reference value for some years, with the number of years that maintain the injectivity linearly increasing with the length of the injection break. The injectivity for an intermittent injection peaks a few years later after the injection starts. Intermittent injections improve the residual and solubility trapping by up to 15% only in the first few years of injection, but the differences in trapping efficiencies among all the injections are within a few percent in the long term. Therefore, the intermittent injections would be useful for a CO_2 storage project to make the best use of a reservoir in 5–10 years under the injection pressure restrictions.

Keywords: CO_2 storage; injectivity; intermittent injection; saline aquifers; trapping efficiency

Introduction

To mitigate global warming, carbon capture from point sources (e.g., power plants) and storage in a particular site (CCS) is one of the most promising options that could significantly reduce greenhouse gas emissions to the atmosphere.[1–3] Deep geological formations, such as saline aquifers, depleted oil and gas fields, or unmineable coal beds, are usually the major target sites for carbon dioxide (CO_2) storage.[4] On the global level, deep saline aquifers are estimated to have a storage potential between 1000 and 10 000 billion tonnes of CO_2 (Gt CO_2) due to their widespread availability, which is much higher than

Correspondence to: Luming Shen, School of Civil Engineering, The University of Sydney, NSW 2006, Australia.
E-mail: luming.shen@sydney.edu.au
Received March 23, 2019; revised April 30, 2019; accepted May 3, 2019
Published online at Wiley Online Library (wileyonlinelibrary.com). DOI: 10.1002/ghg.1888

depleted oil and gas fields (675–900 Gt CO_2) and unmineable coal beds (3–200 Gt CO_2).[5] At present, only saline aquifers and depleted oil and gas fields have successful demonstrations of CO_2 storage at pilot or commercial scales.[6]

CO_2 storage in aquifers involves four trapping mechanisms that take effect on very different time scales.[5] Currently, the most widely used methods of estimating storage capacity in aquifers only consider structural trapping and residual trapping.[7–10] In these methods, the overall storage capacity of the aquifer is estimated with the product of pore volume in the aquifer, *in situ* CO_2 density, and an efficiency coefficient, which takes account of the influence of some factors on storage, such as reservoir heterogeneity, CO_2 buoyance, and mobility.

However, merely assessing storage capacity is not enough for CO_2 storage in an aquifer reservoir. Another crucial factor is that injectivity must also be evaluated. Injectivity describes the ease with which CO_2 can be injected into the aquifer and is defined as the injection rate divided by the pressure difference between the injection well and the reservoir.[5] Reservoir pressure varies dynamically with the injection process, so injectivity is time-dependent and can be influenced by the injection itself.[11] The pressure buildup in the reservoir has large impact on injectivity: the higher the reservoir pressure buildup, the lower the injectivity.[12] For CO_2 storage, the injection process lasts for a limited time period, so insofar as restrictions on maximum pressure buildup limit injection rate, injectivity actually influences the storage capacity. To maximize the CO_2 storage capacity into a given reservoir during a limited period, techniques that reduce the reservoir pressure buildup, such as brine extraction before injection and variable injection rates, have been proposed and studied in numerical simulations.[12–16]

Brine withdrawal is consistently found to be very effective at controlling serious pressure buildup and for maintaining a desired injectivity for large-scale CO_2 injection in saline aquifers, but this type of pressure control would cause the additional environmental problem of brine water disposal. Continuous injection with varying injection rates was found to have no significant effects on the overall pressure buildup in several studies,[12,17–19] but it was suggested that it may influence the injectivity and storage capacity.[19]

Another effective way to control the pressure buildup in the reservoir is simply shutting off the injection periodically.[20] An intermittent injection schedule, i.e., one with breaks in injection, could be designed to improve storage capacity;[21] for example, Bannach *et al.*[19] found that a variable injection rate has the most influential effects in the first year of injection. Ngoc *et al.*[21] suggested that, under the restriction of reservoir pressure buildup in the Bécancour deep saline aquifers in Canada, a 5-year intermittent injection alternating every half a year resulted in maximum storage. Li *et al.*[22] suggested that the increasing injectivity over time observed in the Shenhua Demonstration CCS Project was likely due to intermittent injection.

Furthermore, imbibition, i.e., the process of water displacing CO_2, was often considered as an important trapping mechanism in the postinjection period to assess storage safety, but its effects on injectivity and trapping efficiency, when injection is alternated with breaks, remain largely unknown. Although Ngoc *et al.*[21] and Li *et al.*[22] showed promising results using intermittent injections to improve injectivity, it is uncertain whether their findings are relevant for large-scale storage. Neither was the long-term trapping efficiency considered in those studies. Therefore, a generic reservoir tested with different injection scenarios is needed to investigate the effects of injection procedure on injectivity and trapping efficiency.

The aim of this study is to test different injection-rate scenarios for a single-well injection in a synthetic saline aquifer for CO_2 storage over 100 years against injectivity and storage efficiency through numerical simulations. A parametric study was conducted to investigate the influences of key factors, including reservoir compressibility, boundary conditions, permeability distribution features, capillary pressure, and relative permeability curves, on the effectiveness of these injection scenarios against injectivity and trapping efficiency. The purpose is to assist injection strategy design to improve injectivity and trapping efficiency for a large-scale storage project by optimizing the injection scenarios, which may help in cost cutting and reducing environmental impacts.

Methods

Characteristics of reservoir and operation

The synthetic saline aquifer used for different injection scenarios was assumed to be horizontal with the injector in the center, and with a 20 km radius and 30 m thickness with the top at the depth of 1485 m underground (Fig. 1(a)). The formation pressure gradient was assumed to be 9.81 kPa m^{-1}; the

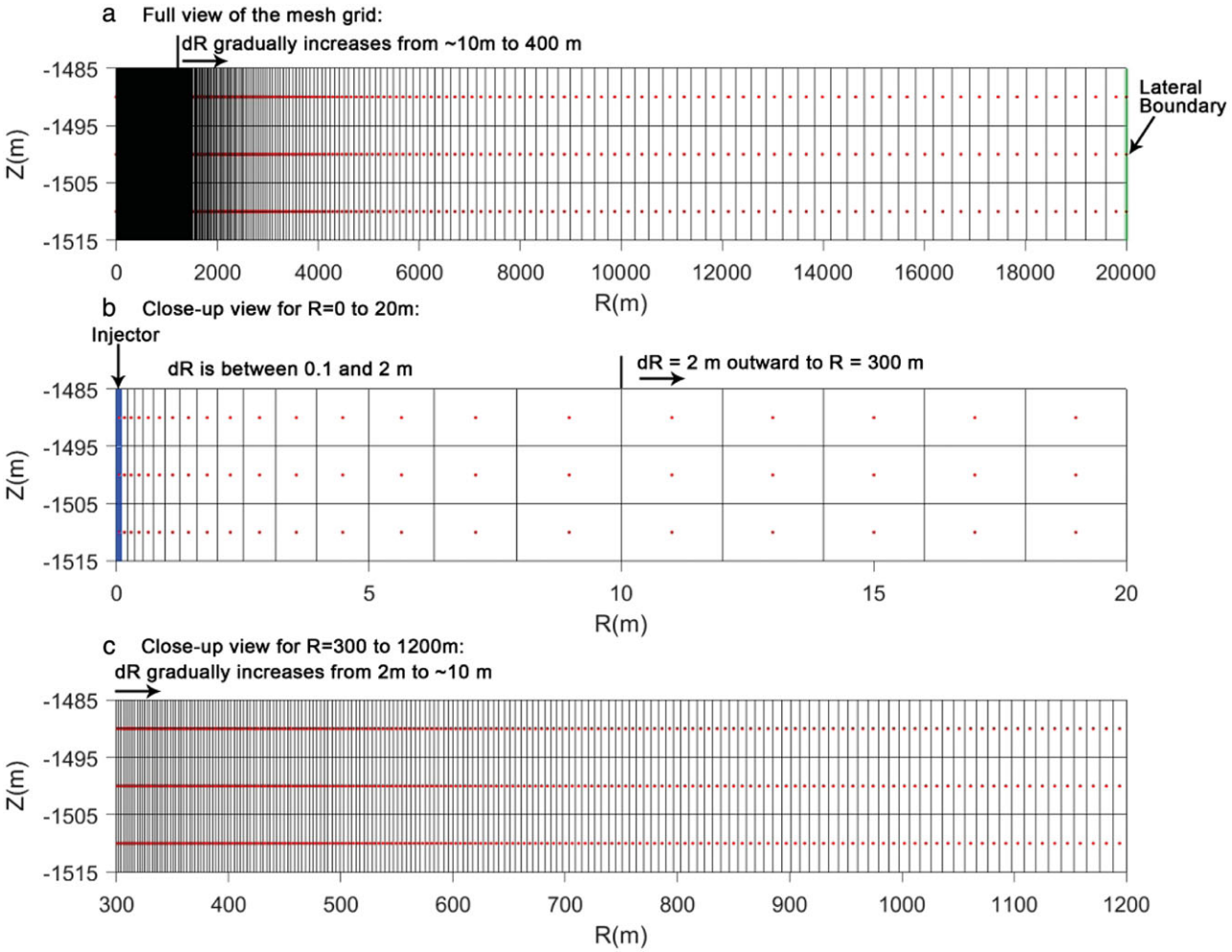

Figure 1. Model setup and discretization presented in 2D axisymmetric way (a red dot represents the center of a grid block).

geothermal gradient was 0.03°C m^{-1}. The formation porosity was 25%. Both horizontal and vertical formation permeabilities were 1.0×10^{-12} m^2. Aquifer pore compressibility was 1.0×10^{-10} Pa^{-1}. The model was initially 100% saturated with brine at 1.5% salinity by mass fraction.

With an assumption that one million tonnes of CO_2 must be injected yearly into the reservoir for 30 years, the injection scenarios included a constant injection at 32.15 kg s^{-1} as the base scenario, and three intermittent injections that cycled yearly as (1) 1-month injection at 64.3 kg s^{-1} alternated with a 1-month break, six times in a year; (2) 1-month injection at 192.90 kg s^{-1} alternated with a 5-month break, twice a year; and (3) 1-month injection at 385.8 kg s^{-1} followed by an 11-month break (Fig. 2). For all the scenarios, the simulation was run for 100 years, including the first 30 years for injection and 70 years of postinjection period. Because intermittent injection would give rise to frequent alternations between drainage and wetting processes in the reservoir, hysteretic effects of capillary pressure and relative permeability were considered in simulation.

Modeling approach

TOUGH2 with the ECO2N module integrated with hysteretic capillary pressure and relative permeability functions in the parallel version was used for the simulations in this study.[23–26] TOUGH2–ECO2N is a numerical simulator for nonisothermal fluids composed of H_2O, NaCl, and CO_2 in a water-rich aqueous phase (liquid) and a CO_2-rich gas phase (gas) in porous media. Solid salt may also be present in the geochemical system. TOUGH2–ECO2N includes a comprehensive description of thermodynamic and

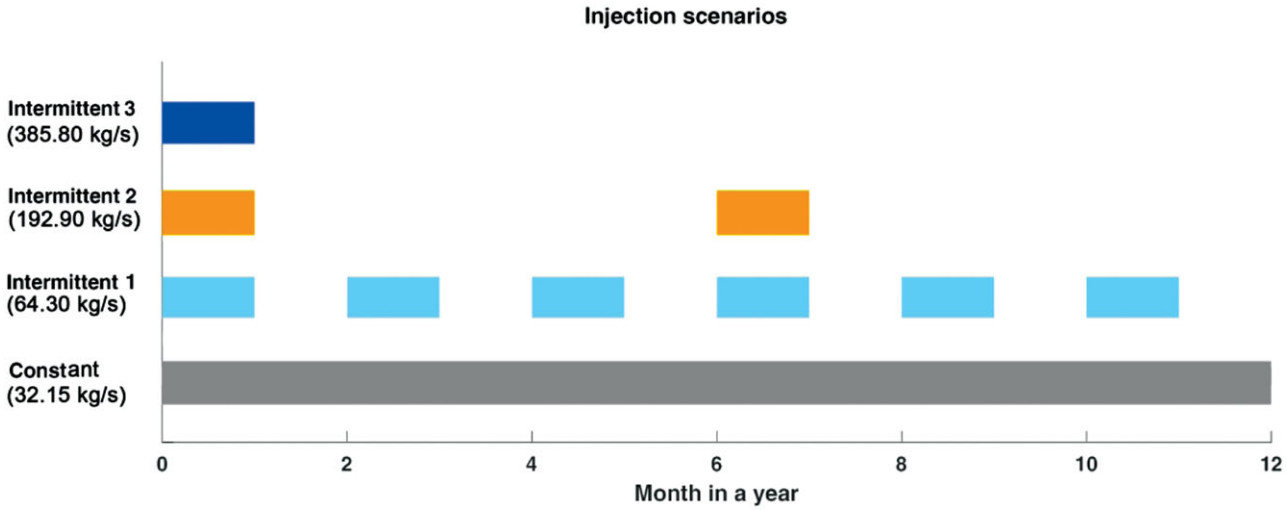

Figure 2. Yearly injection sequence for the four injection scenarios.

physical properties of H_2O–NaCl–CO_2 mixtures within experimental error for temperature between 10 and 110°C, pressure up to 60 MPa, and salinities ranging from 0 to saturation. Density, viscosity, and specific enthalpy of the fluid phases used in modeling water–salt–CO_2 mixtures in porous media are functions of temperature, pressure, composition, and partitioning of components among the phases. Detailed description and equations used in the ECO2N module can be found in Pruess[24] and are not repeated here.

Capillary pressure was described with the van Genuchten[27] equation adapted by Doughty[25] to account for hysteresis expressed by

$$P_c = -P_0^p \left[\left(\frac{S_l - S_{l\min}}{1 - S_{gr}^{\Delta} - S_{l\min}} \right)^{-\left(\frac{1}{mp}\right)} - 1 \right]^{(1-mp)}, \quad (1)$$

where P_c is capillary pressure, P_0 is capillary strength coefficient, p identifies drainage (d) or imbibition (w) process, S_l is liquid saturation, $S_{l\,\min}$ is saturation at which original van Genuchten P_c goes to infinity, S_{gr}^{Δ} is residual gas saturation, and m is the parameter in van Genuchten.[27] In Eqn (1), the residual gas saturation (S_{gr}^{Δ}) is dependent on the liquid saturation at the turning point of transition from drainage to imbibition, rather than a constant value, and is calculated by

$$S_{gr}^{\Delta} = \frac{1}{1/(1 - S_l^{\Delta}) + 1/S_{gr\max} - 1/(1 - S_{lr})}, \quad (2)$$

where S_l^{Δ} is the turning-point liquid saturation, $S_{gr\max}$ is maximum residual gas saturation, and S_{lr} is residual liquid saturation. Similarly, relative permeabilities to liquid and gas were based on the modified van Genuchten[27] model by Parker and Lenhard[28] and Lenhard and Parker,[29] and are given by

$$k_{rl} = \sqrt{\bar{S}_l}\left[1 - \left(1 - \frac{\bar{S}_{gt}}{1 - \bar{S}_l^{\Delta}}\right)\left(1 - (\bar{S}_l + \bar{S}_{gt})^{1/m}\right)^m - \left(\frac{\bar{S}_{gt}}{1 - \bar{S}_l^{\Delta}}\right)\left(1 - (\bar{S}_l^{\Delta})^{1/m}\right)^m\right]^2 \quad (3)$$

and

$$k_{rg} = k_{rg\max}\left(1 - (\bar{S}_l + \bar{S}_{gt})\right)^{\gamma}\left(1 - (\bar{S}_l + \bar{S}_{gt})^{1/m}\right)^{2m}, \quad (4)$$

respectively, where $\bar{S}_l$ is effective liquid saturation calculated by $\frac{S_l - S_{lr}}{1 - S_{lr}}$, $\bar{S}_l^{\Delta}$ is effective turning-point liquid saturation calculated by $\frac{S_l^{\Delta} - S_{lr}}{1 - S_{lr}}$, $\bar{S}_{gt}^{\Delta}$ is effective trapped gas-phase saturation calculated by $\frac{S_{gr}^{\Delta}(S_l - S_l^{\Delta})}{(1 - S_{lr})(1 - S_l^{\Delta} - S_{gr}^{\Delta})}$, and γ is an exponent parameter. With Eqns (3) and (4), relative permeabilities to liquid and gas can be calculated for both drainage and wetting processes. The only difference is that $\bar{S}_{gt}^{\Delta}$ is zero for drainage but nonzero for wetting when calculating relative permeability to gas. The reader is referred to Doughty[25] for more details.

Model discretization and parameterization

The injector was perforated along the whole reservoir thickness and CO_2 was injected evenly along the

Table 1. Parameters used in the capillary pressure and relative permeabilities equations.

Capillary pressure equations	m^d	0.411	Relative permeability equations	Liquid phase	m	0.917
	S_{lmin}	0.01			S_{lr}	0.25
	$P_0{}^d$ (Pa)	1.189×10^4			S_{grmax}	0.25
	m^w	0.411		Gas phase	γ	2.0
	$P_0{}^w$ (Pa)	1.189×10^4			k_{rgmax}	1.0
	S_{grmax}	0.25			m	0.5

perforation length (Fig. 1(b)). A 2D radial axisymmetric grid was used to discretize the reservoir (Fig. 1(a)). In the horizontal direction, radial grid block sizes gradually varied: from 0.1 and 2 m from the well to a distance of 10 m, then were uniformly 2 m out to a distance of 300 m, then varied from 2 to 10 m out to a distance of 2300 m, then between 10 and 100 m out to a distance of 7000 m, then from 100 to 200 m out to a distance of 10 000 m, and then from 200 to 400 m out to 20 000 m. Then another grid block had a very small extent (0.1 m) from 20 000 m and served as the lateral boundary (Fig. 1(a)). The radius of the reservoir was divided into 502 parts, while the vertical extent into 3 layers with a thickness of 10 m each. Therefore, there were 1506 elements in the model after discretization.

As a preliminary step not detailed here, a mesh convergence study was carried out on a 10 m thick reservoir with a 10 km radius in different radial discretizations. The results showed that a balance between accuracy and computational efficiency was achieved with the mesh applied in Fig. 1.

The reservoir initial pressure was obtained by first applying the pressure gradient of 9.81 kPa m^{-1} to all the grid blocks. Then, after running a gravitational balance calculation by fixing the central layer pressure at 14.7150 MPa, we obtained the initial pressure of the upper layer at 14.6172 MPa, and of the lower layer at 14.8127 MPa.

The reservoir initial temperature was determined by applying the geothermal temperature gradient of 0.03°C m^{-1} with the ground surface temperature at 20°C. Therefore, the initial temperature of the layers from top to bottom was 64.7, 65, and 65.3°C, respectively.

The reservoir was initially saturated with NaCl brine at 1.5% mass fraction. The upper, lower, and outer model boundaries were assumed to be closed to flow. The grid blocks that represent the injection well were assigned an infinite rock grain density (2.6×10^{40} kg m^{-3}) to ensure that CO_2 injection would effectively occur at the grid block initial temperature.

The parameters in the models of capillary pressure curve and relative permeabilities were taken from Doughty,[36] representing a sandstone suitable for CO_2 storage (see Table 1).

Other assumptions made for simulation include the following: (1) the top and bottom layers of the model were bounded with impermeable formations; (2) injection is an isothermal process; (3) except for CO_2 dissolution in water, chemical reactions between rock, water, and CO_2 were not considered due to a relatively short simulated timescale; (4) solid salt present in pores due to CO_2 injection would not affect permeability; and (5) CO_2 injection did not cause any mechanical deformations in the reservoir.

Sets of simulation cases

First, the four injection scenarios were applied to the reservoir with the settings described previously to investigate the reservoir responses. These four cases were grouped as the base set. Then, other seven sets of cases were designed for a parametric analysis to investigate sensitivity of reservoir responses to several variables. The considered reservoir characteristics included formation compressibility, type of boundary condition, permeability distributions, and capillary pressure and relative permeability characteristic curves (see summary in Table 2). Figure 3 illustrates the permeability distributions for sets 3–6. Figure 4 shows the different characteristic curves of relative permeabilities to gas and liquid and of capillary pressure used in the base set and Set 7. Set 7 was set to investigate how a reservoir would respond if capillary pressure and relative permeability characteristics curves were more favorable to CO_2 movement. Set 7 had a reduced capillary strength coefficient (P_0), a smaller gas residual saturation, and a smaller van Genuchten m for the liquid relative permeability.

Table 2. Summary of simulation case sets based on reservoir characteristics.

Case set	Reservoir compressibility (Pa^{-1})	Boundary conditions	Permeability distribution	Key parameters in the capillary pressure function	Key parameters in the relative permeability function
Base	1.0×10^{-10}	All closed	Homogeneous and isotopic, $k = 1.0 \times 10^{-12}$ m^2	$\lambda = 0.411$, $P_0 = 11\,890$ Pa $S_{lr} = 0.25$, $S_{grmax} = 0.25$, $S_{lmin} = 0.01$	$m^l = 0.917$, $S_{lr} = 0.25$; $S_{grmax} = 0.25$, $\gamma = 2.0$ $k_{rgmax} = 1.0$, $m^g = 0.5$
Set 1	1.0×10^{-9}	Same as base	Same as base	Same as base	Same as base
Set 2	Same as base	Pressure on the lateral boundary is constant as the initial pressure*	Same as base	Same as base	Same as base
Set 3	Same as base	Same as base	Heterogeneous and isotropic, linearly decreasing from 2.0×10^{-12} m^2 at the injector to 0.5×10^{-12} m^2 at the outer boundary, $\bar{k} = 1.0 \times 10^{-12}$ m^2	Same as base	Same as base
Set 4	Same as base	Same as base	Heterogeneous and isotropic, linearly increasing from 0.5×10^{-12} m^2 at the injector to 1.25×10^{-12} m^2 at the outer boundary, $\bar{k} = 1.0 \times 10^{-12}$ m^2	Same as base	Same as base
Set 5	Same as base	Same as base	Heterogeneous and isotropic, randomly distributed between 0.5×10^{-12} m^2 and 2.0×10^{-12} m^2, $\overline{k} = 1.0 \times 10^{-12}$ m^2, $s = 0.1 \times 10^{-12}$ m^2	Same as base	Same as base
Set 6	Same as base	Same as base	Heterogeneous and isotropic, randomly distributed between 0.5×10^{-12} m^2 and 2.0×10^{-12} m^2, $\bar{k} = 1.0 \times 10^{-12}$ m^2, $s = 0.3 \times 10^{-12}$ m^2	Same as base	Same as base
Set 7	Same as base	Same as base	Same as base	$\lambda = 0.411$, $P_0 = 5945$ Pa $S_{lr} = 0.25$, $S_{grmax} = 0.15$, $S_{lmin} = 0.01$	$m^l = 0.817$, $S_{lr} = 0.25$; $S_{grmax} = 0.15$, $\gamma = 2.0$ $k_{rgmax} = 1.0$, $m^g = 0.5$

*This is achieved by increasing the volume of the lateral boundary grid blocks to infinite (10^{50} m^3).

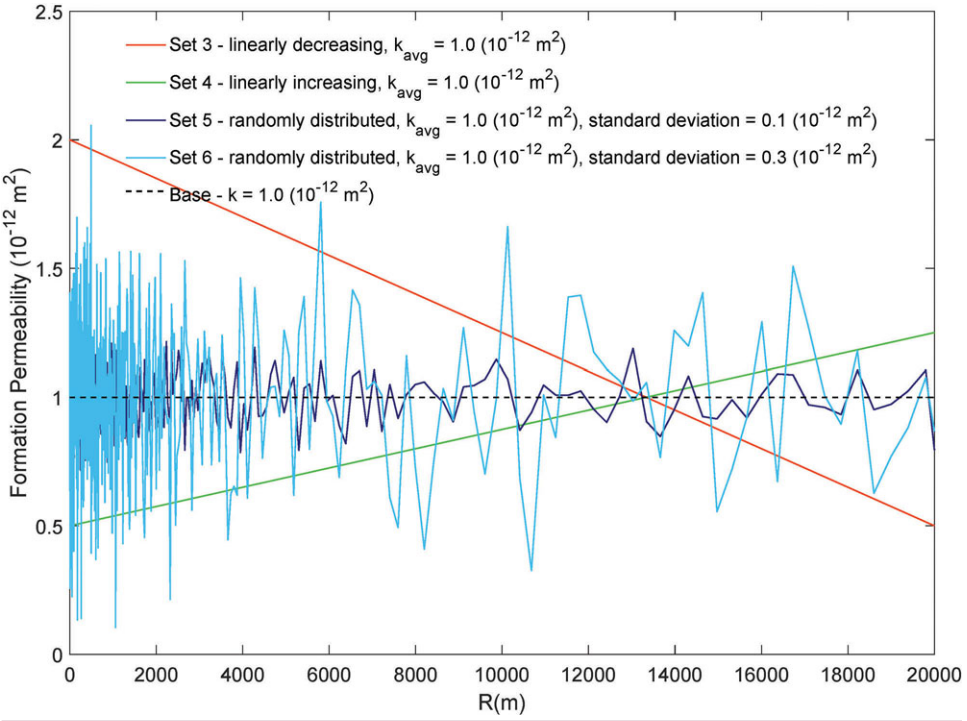

Figure 3. Formation permeability distributions for Sets 3–6 for the parametric analysis.

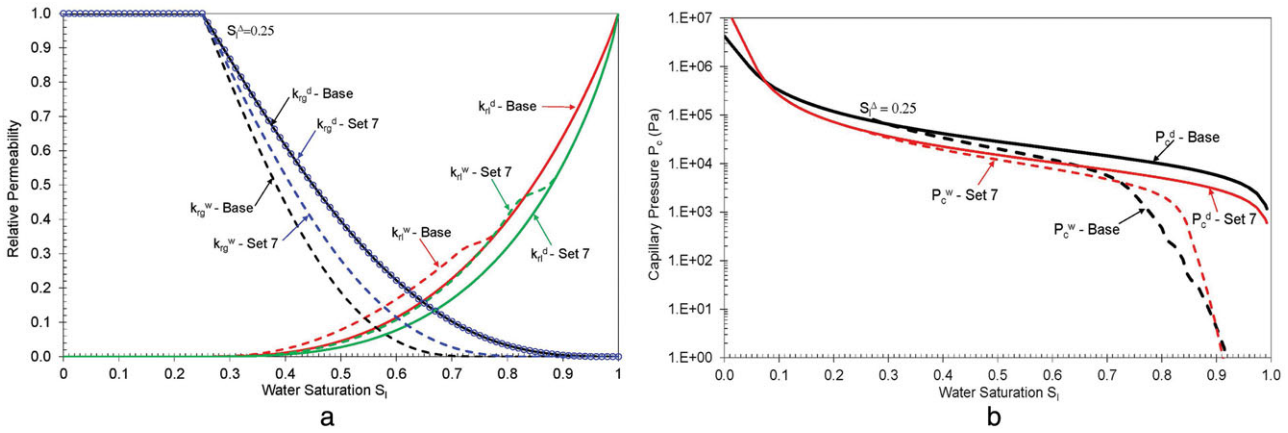

Figure 4. (a) Gas and liquid relative permeability curves for drainage (k^d_{rg} and k^d_{rl}) and imbibition (wetting, assuming the turning point right at when water saturation is 0.25) (k^w_{rg} and k^w_{rl}) processes used for base set and Set 7; (b) capillary pressure curves for drainage (P^d_c) and imbibition (wetting, assuming the turning point right at when water saturation is 0.25) (P^w_c) process used for base set and Set 7 (P_c curves were extended for $S_l < S_{lr}$ with functions by Doughty[25]).

Reservoir response assessment

Reservoir responses to the different injection scenarios were assessed against injection pressure, pressure buildup, injectivity, and trapping efficiency. We chose these four criteria based on the considerations as follows. Injection pressure design and limitations are usually based on several considerations. For example, the reservoir should not be fractured or damaged under the injection pressure, the brine in the area affected by injection pressure should be free of risk of being lifted to shallower fresh aquifers, the caprock integrity should be maintained under the elevated pressure, and economic concerns about operational energy costs should also be taken into consideration. When injection rate and injection duration were decided, the operator needs to preassess the consequential injection pressure and any risk of the injection pressure that would impose on caprock

integrity. Pressure buildup in the reservoir reflects reservoir dynamics through pressure propagation in the reservoir. Injectivity indicates the ease of injection operation and storage capacity during the injection years. Trapping efficiency is about CO_2 storage viability and indicates storage efficiency. These factors together allow a comprehensive assessment of the reservoir responses to the injection process.

Injection pressure is the pressure at the injector during injection period. Pressure at any location in the reservoir was calculated by the simulation tool we used. As the injector was represented by three grid blocks (Fig. 1(b)), the injection pressure in the assessment uses the mean of the pressure at these three grid blocks, which is given by

$$P_{t,inj} = (P_{t,wellblock1} + P_{t,wellblock2} + P_{t,wellblock3})/3, \quad (5)$$

where $P_{t,inj}$ is injection pressure at time t during an injection period, $P_{t,wellblock1}$, $P_{t,wellblock2}$, and $P_{t,wellblock3}$ are the pressure at the same time at the three grid blocks that make up the injection well, respectively. Pressure is calculated at each time step (P_t, up to 1 h) during simulation, so the daily mean injection pressure of a single injection day (injection rate >0) is calculated by

$$\begin{aligned}\bar{P}_{day_i,inj} &= \frac{1}{n}\sum_{j=1}^{n} P_{t_j,inj} \\ &= \frac{1}{3n}\sum_{j=1}^{n} (P_{t_j,wellblock1} + P_{t_j,wellblock2} \\ &\quad + P_{t_j,wellblock3}), \end{aligned} \quad (6)$$

where $\bar{P}_{day_i,inj}$ is daily mean injection pressure of injection day i (*when injection rate* > 0), n is the number of time steps that elapse on that day, and $P_{t_j,inj}$ is injection pressure at time step j on that day. The annual mean injection pressure of an injection year is calculated by

$$\bar{P}_{year_i,inj} = \frac{1}{m}\sum_{j=1}^{m} \bar{P}_{day_j,inj}, \quad (7)$$

where $\bar{P}_{year_i,inj}$ is annual mean injection pressure of injection year i, m is the number of the injection days (total number of the days when injection rate > 0) in that year, and $\bar{P}_{day_j,inj}$ is daily mean injection pressure of injection day j in that year. Similarly, the average annual injection pressure over the 30 years for each scenario can be obtained by

$$\bar{P}_{inj} = \frac{1}{30}\sum_{j=1}^{30} \bar{P}_{year_j,inj}, \quad (8)$$

where $\bar{P}_{inj}$ is average annual injection pressure.

The pressure buildup at a specific time and location is defined as the pressure difference between current and initial pressure at that location, and is given by

$$\Delta P_{t,l} = P_{t,l} - P_{0,l}, \quad (9)$$

where $\Delta P_{t,l}$ is the pressure buildup at time t at location l, $P_{t,l}$ is the pressure at time t at location l, and $P_{0,i}$ is the initial pressure at location l. So, the time-dependent pressure buildup over the distance from the injector indicates the pressure propagation across the reservoir.

Injectivity represents the CO_2 flow into the reservoir under a unit pressure difference between the injector and the aquifer per unit length of injector perforation, and is expressed by Law and Bachu[30]

$$I = \frac{Q}{D}/(P_{inj} - P_a), \quad (10)$$

where I is the injectivity ((ton/day)/(MPa/m)), Q is the injection mass rate (ton day^{-1}), D is aquifer thickness (m), P_{inj} is the injection pressure (MPa) t, and P_a is aquifer pressure (initial pressure) (MPa) at the injector before injection starts. With Eqn (10) and Eqns (5)–(8), injectivity at every time step (I_t), daily mean injectivity ($\bar{I}_{day}$) of an injection day, annual mean injectivity ($\bar{I}_{year}$) of an injection year, and the average annual injectivity ($\bar{I}$) of 30 injection years for a scenario can be calculated accordingly.

Given the assumptions that the reservoir was overlaid by an impermeable caprock and there was no CO_2 mineral trapping, the trapping efficiency in this study only included the residual and solubility trapping, which are represented by the mass fractions of immobile gaseous and aqueous CO_2 in the reservoir, respectively. The higher the mass fraction of immobile gaseous CO_2, the higher the residual trapping efficiency. Dissolution of CO_2 into the brine will slightly increase the brine density, so the CO_2-dissolved brine will move downward. This would increase not only the CO_2 storage security but also the storage capacity because higher brine density means lower volume of aqueous phase CO_2 and, therefore, a larger reservoir storage volume. Hence, a higher aqueous CO_2 mass fraction also indicates a higher

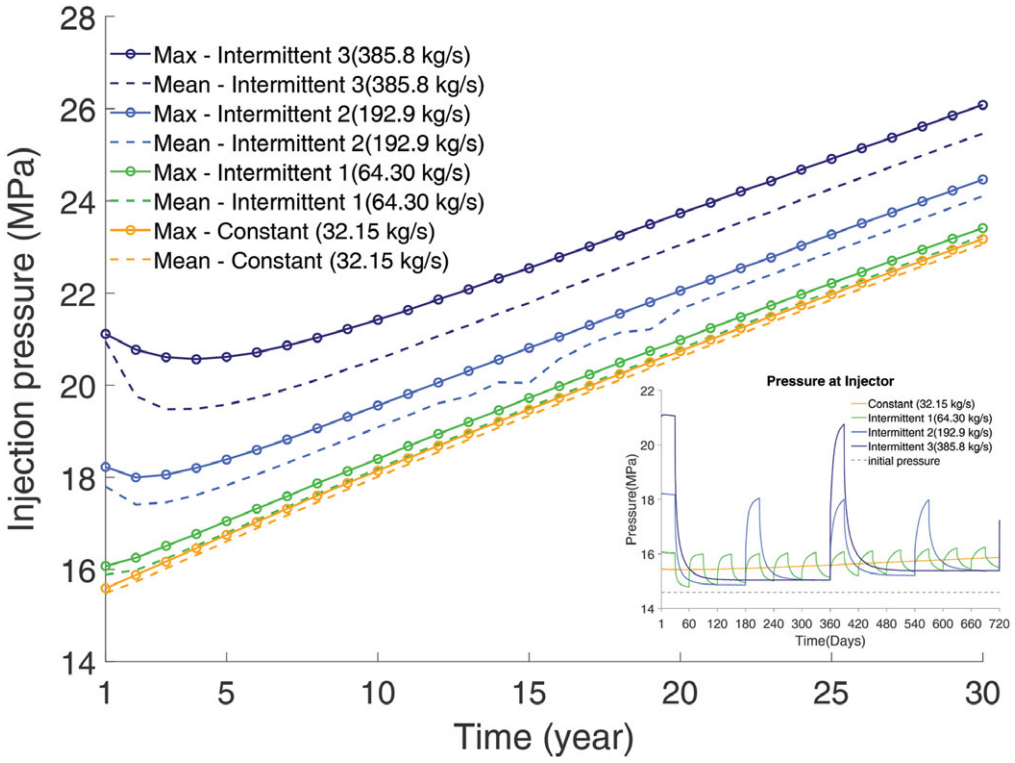

Figure 5. Annual maximum and mean injection pressure for different injection scenarios with an inset of daily mean pressure variation at the injector within the first 720 days.

trapping efficiency. So, the trapping efficiency in this study is expressed by the sum of residual trapping and solubility trapping. The residual trapping is the ratio of the mass of gaseous CO_2 whose gas saturation is equal to or below the residual gas saturation to the total injected CO_2 mass at a time. The solubility trapping is the ratio of the aqueous CO_2 mass to the total injected CO_2 mass at a time.

Results and discussion

Injection pressure and pressure buildup of the reservoir

Figure 5 shows the annual maximum injection pressure (the maximum injection pressure occurs in a year) and the annual mean injection pressure for different injection scenarios. Constant injection shows a monotonic increase in the annual mean injection pressure from 15.5 to 23.1 MPa over the years, while the intermittent injections have a decrease in the first several years and an upward trend afterward. The intermittent injections always have a higher annual mean injection pressure than the constant injection for the same year, but such injection pressure differences decrease over the years. Over the injection years, differences in the annual mean injection pressure for the intermittent-injection scenarios 1–3 from that for the constant-injection scenario decrease from 0.41 to 0.18 MPa (2.63–0.79%), from 2.32 to 1.04 MPa (14.96–4.52%), and from 5.46 to 2.40 MPa (35.28–10.41%), respectively. After 5 years, these annual mean injection pressure differences are relatively stable at about 0.18 MPa (0.90%), 1.03 MPa (5.16%), and 2.50 MPa (12.54%), respectively.

The higher annual mean injection pressure required by the intermittent-injection scenarios indicates that the injection breaks are not as effective as expected to help controlling the injection pressure. The inset in Fig. 5 shows that, even in the first year, the pressure drop at the injector after an injection break is not enough to take the pressure at the injector back to the initial level. Over the injection years, pressure drops at the injector over the injection breaks for these intermittent-injection scenarios gradually decrease.

The highest injection pressure needs to be assessed for injection safety and to satisfy restrictions on injection operation. To avoid breaking the caprock and creating potential paths for CO_2 leakage, the highest

  | *Greenhouse Gas Sci Technol*. **9**:652–671 (2019); DOI: 10.1002/ghg

injection pressure must not exceed the highest permissible pressure, which is usually recommended as 10–20% below the fracture pressure of the aquifer. It is challenging to calculate fracture pressure gradient without logging data from boreholes. Previous studies show that the fracture pressure for a sedimentary rock is usually between 1.75 and 2.25 times of the initial formation pressure at the same depth.[31–33] In this study, the highest injection pressure is the annual maximum pressure of Year 30. If we assumed the fracture pressure of the reservoir to be twice the initial pressure and the safety coefficient to be 0.85 (15% below the fracture pressure), the highest permissible pressure would be 25.02 MPa at 1500 m depth. All of the scenarios would be regarded as safe except intermittent-injection scenario 3, whose highest injection pressure is 1 MPa higher than the assumed highest permissible pressure. If we used the same safety coefficient but the lower limit (1.75) for fracture pressure estimate, the highest permissible pressure would be 21.89 MPa. In this case, intermittent-injection scenarios 2 and 3 would exceed allowable pressure after 23 and 12 years, respectively.

Figure 6(a) displays the pressure buildup in the reservoir for the different injection scenarios. The pressure buildup for the constant injection steadily increases with time, while the pressure buildup for the intermittent injections changes substantially between injection days and injection breaks. During the injection days, the pressure buildup for an intermittent injection is more intense than that of the constant injection. The more intense pressure buildup always occurs within a certain distance from the injector (Fig. 6(b)), while beyond this distance the pressure buildup for the intermittent injections becomes lower than that for the constant injection. This distance indicates the different influence area due to different injection durations. For CO_2 storage in aquifers, pressure buildup travels far more quickly than CO_2 plume,[34] so the influence distance can be calculated by $L = 2\sqrt{\pi kt/(\phi C\mu)}$, where k is permeability (m^2), t is time (s), ϕ is porosity, C is sum of water compressibility and rock compressibility (Pa^{-1}), and μ is water viscosity (Pa·s). Given the water compressibility at 15 MPa and 65°C being about 4.25×10^{-10} Pa^{-1} [35] and water viscosity being 0.5×10^{-3} Pa·s with 1.5% NaCl mass fraction, the influence distance for 1 month injection is about 7 km, and for 1 year is about 20 km. So, the pressure buildup beyond 7–10 km from the injector for an intermittent injection is lower than that for the constant injection.

Injectivity

Figure 7 compares the annual mean injectivity ((ton/d)/(MPa/m)) of some years across the different injection scenarios. It was found that differences in the injectivity between the scenarios grow with time. The first-year annual mean injectivity for the constant injection is 130 (ton/d)/(MPa/m), and for the intermittent-injection Scenarios 1–3 is 140, 160, and 175 (ton/d)/(MPa/m), respectively. However, over the following 29 years, the injectivity for the constant injection declines quickly (dropping by about 8% per year), while the intermittent injections maintain a relatively high injectivity for several years. Taking the first-year annual mean injectivity for the constant injection as the reference, intermittent-injection Scenarios 1–3 maintain the injectivity above the reference for 3, 10, and 21 years, respectively. Taking the first-year annual injectivity for each intermittent injection itself as the reference, intermittent injections 1–3 maintain the injectivity above their corresponding reference for 2, 5, and 12 years, respectively. The number of years that the injectivity is maintained above a given reference value by an intermittent injection linearly increases with the length of the injection break (Fig. 8).

The results indicate that the annual mean injectivity of an intermittent injection would peak in a few years after the injection started. This implies that an intermittent injection could have a rising injection rate in some years if the injection is operated with fixed injection pressure. This is especially helpful in practice to optimize an injection plan that needs to make the best use of the reservoir in a relatively short period under a certain pressure. Our results are consistent with those in Ngoc *et al.*,[21] who showed that a 5-year intermittent-injection scenario achieved a maximum storage of CO_2 in a specific reservoir under the pressure restriction. Similar findings were also reported in the Shenhua Demonstration CCS Project.[22] Though Li *et al.*[22] did not discuss the injectivity variation later than 3 years, it could be predicted here that the injectivity would not keep increasing if the injection would have continued after 3 years.

Trapping efficiency

Figure 9 shows that the intermittent injections have a prominently higher trapping efficiency than the constant injection in the first year, but no significant differences in the trapping efficiency at the ends of 30

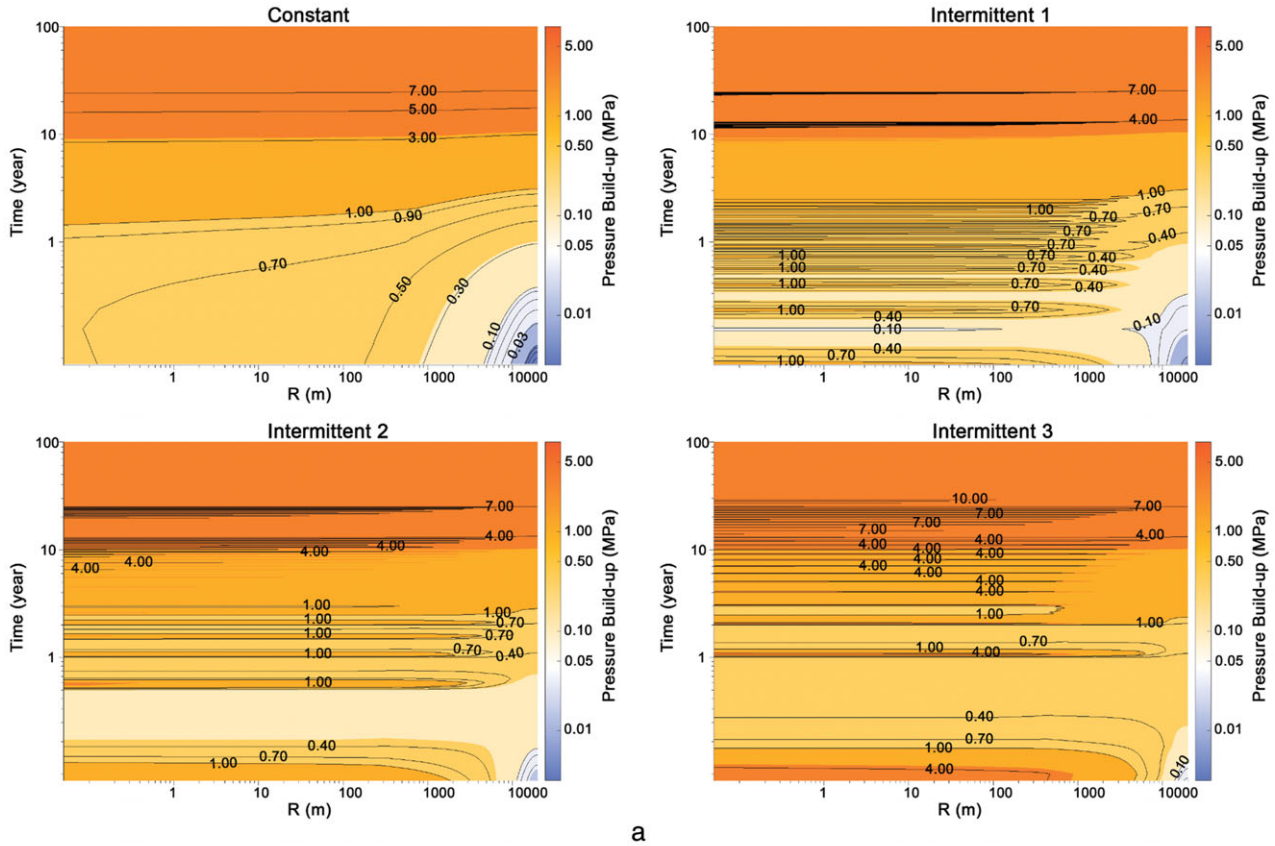

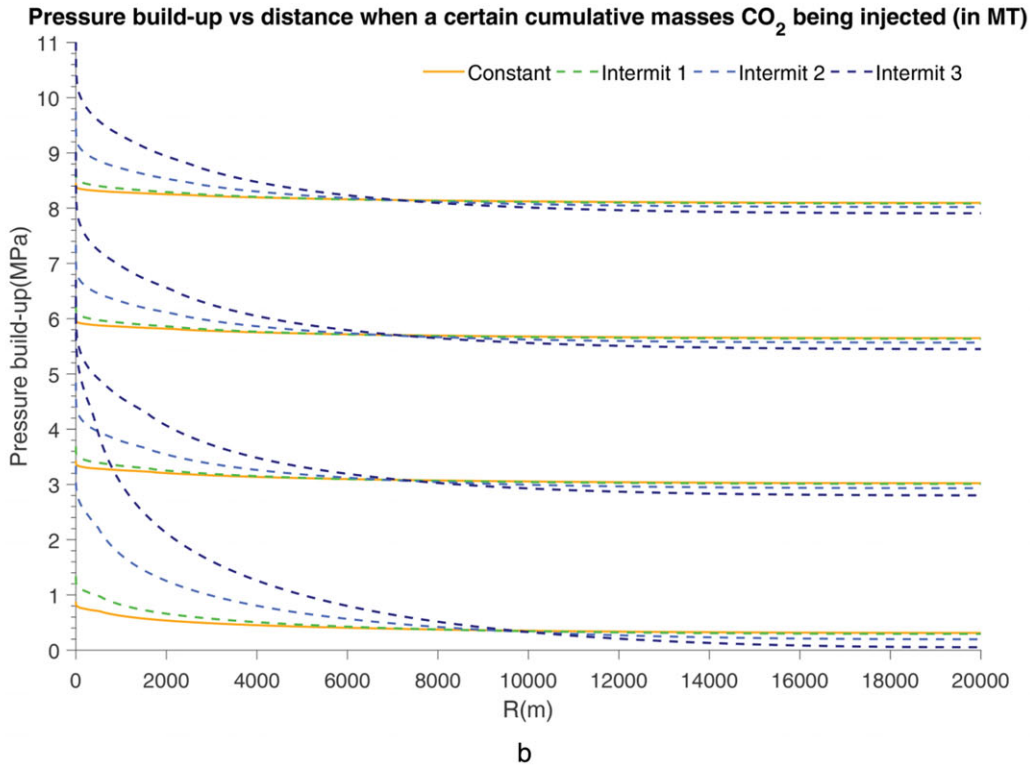

Figure 6. (a) Pressure buildup variations over the distance from the injector and time; and (b) pressure buildup varying with the distance from the injector for a certain cumulative mass (in MT) of CO_2 being injected.

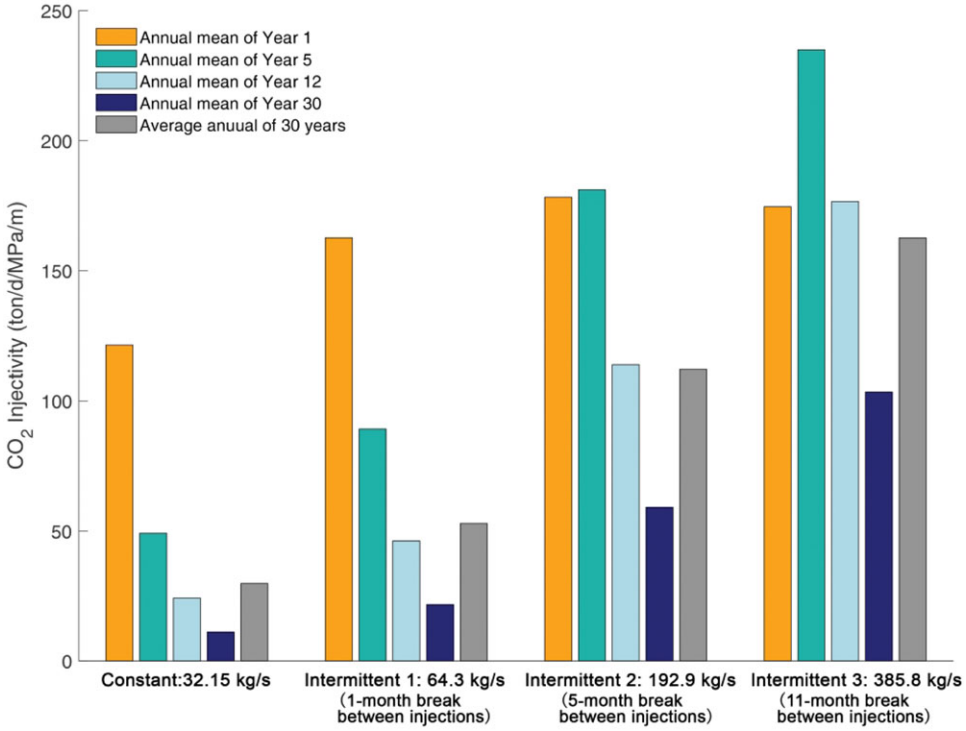

Figure 7. Comparison of the annual mean injectivity of some years and average annual injectivity between the injection scenarios.

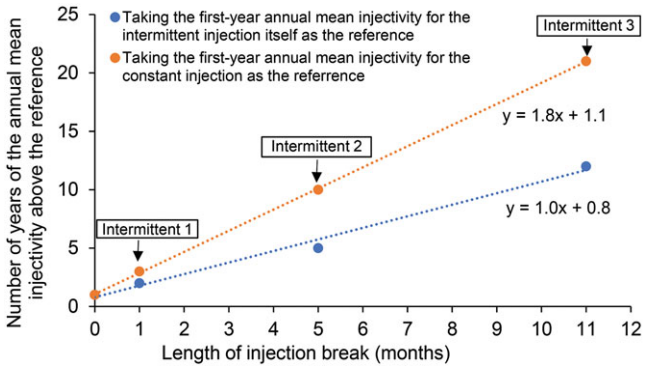

Figure 8. Relationship between the number of years of the annual mean injectivity above the reference and the length of injection break for the intermittent-injection scenarios.

and 100 years. In the first year, the mass fraction of immobile CO_2 gas for an intermittent injection could be 13% higher than that for the constant injection, indicating that a much higher trapping efficiency for this year is due primarily to residual trapping. However, this gain in trapping efficiency for the intermittent injections quickly decreases in later years. The trapping efficiency at the end of 5 years (not shown in Fig. 9) for these scenarios is close. The reason for the differences in residual trapping between these injection scenarios is likely due to the time lag between imbibition and maximum CO_2 gas saturation achieved before imbibition starts. Generally, no significant imbibition is expected to occur during injection unless the injection stops.[36] So, at the end of the first year, the intermittent-injection scenarios 1–3 have experienced significant imbibition for 6, 10, and 11 months, while the constant injection went through no significant imbibition. Thus, prominently higher residual trapping is seen in the intermittent-injection scenarios. On the other hand, based on Land[37] and Krevor *et al.*,[38] the higher the CO_2 gas saturation achieved before imbibition starts, the more CO_2 gas will be trapped during the imbibition process. The maximum CO_2 gas saturations achieved in the intermittent injections decrease with the times of imbibition and drainage alternating with one another because a new drainage process (injection) would remobilize the CO_2 trapped from previous imbibition. Therefore, after several cycles of drainage and imbibition, residual trapping becomes less and less significant for the intermittent injections. As a result, all injection scenarios have a similar CO_2 gas saturation at the end of 30 years. Once the injection stops permanently, significant imbibition

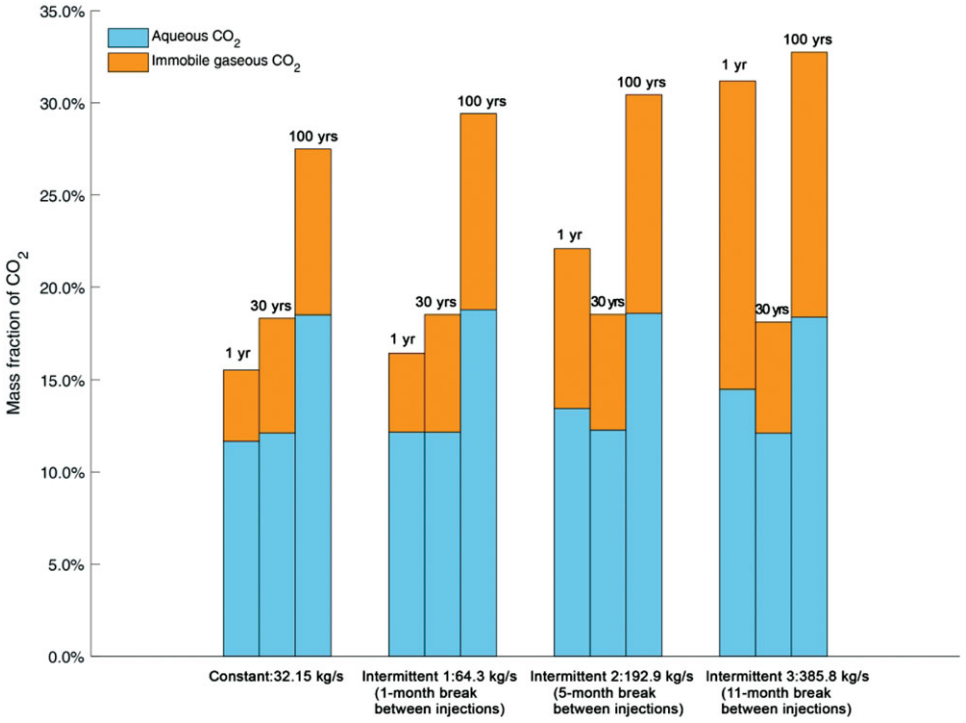

Figure 9. Trapping efficiency at the ends of 1, 30, and 100 years for the injection scenarios.

starts to occur across all injection scenarios, and therefore, residual trapping efficiencies with only a few percentage differences among these scenarios are observed at the end of 100 years.

Doughty[39] suggested that there would be an interesting trade-off between residual trapping and CO_2 dissolution. The more extensively the CO_2 plume spreads before being immobilized by residual trapping, the more dissolution of CO_2 into the brine there will be.[40] In this study, both a higher residual trapping and a higher mass fraction of aqueous CO_2 are observed for the intermittent injections in the first year. This higher solubility trapping is mainly caused by a higher pressure around the injector for the intermittent injections compared to the constant-injection scenario.

In conclusion, apart from the first few years, the intermittent injections would not result in a trapping efficiency significantly different from that of a constant injection.

Parametric study

Figure 10 compares the maximum injection pressure of Year 30 (the highest injection pressure) for the injection scenarios across the different reservoir settings. The injection pressure is compared for the same injection scenario between sets 1 and 7 and the base set. We found that the highest injection pressure for all the injection scenarios is much lower in Set 1 (reservoir compressibility 10 times higher) and Set 2 (pressure at the lateral boundary is constant) than that in the base set. Set 5 (permeability is randomly distributed with the same average permeability and a standard deviation of 10% average permeability), Set 6 (permeability is randomly distributed with the same average permeability and a standard deviation of 30% average permeability), and Set 7 (capillary pressure strength is reduced by 50% and gas residual saturation decreases by 40%) have the highest injection pressure for all the injection scenarios close to that in the base set. In Set 3 (permeability linearly decreases from 2×10^{-12} m^2 at the injector to 0.5×10^{-12} m^2 on the boundary) and Set 4 (permeability linearly increases from 0.5×10^{-12} m^2 at the injector to 1.25×10^{-12} m^2 on the boundary), only the constant and Intermittent 1 injections have the highest injection pressure close to that in the base set. The highest injection pressure for the intermittent-injection scenarios 2 and 3 in Set 3 is prominently lower than that in the base set, but in Set 4 it is conspicuously higher than that in the base set. If fracture pressure was assumed to be double the initial pressure, although no

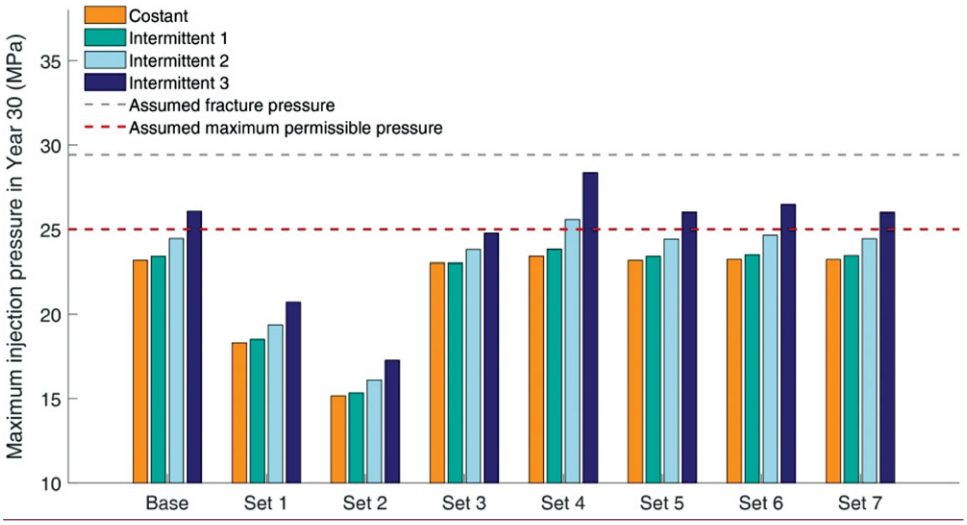

Figure 10. The maximum injection pressure in Year 30 for the injection scenarios across different reservoir settings.

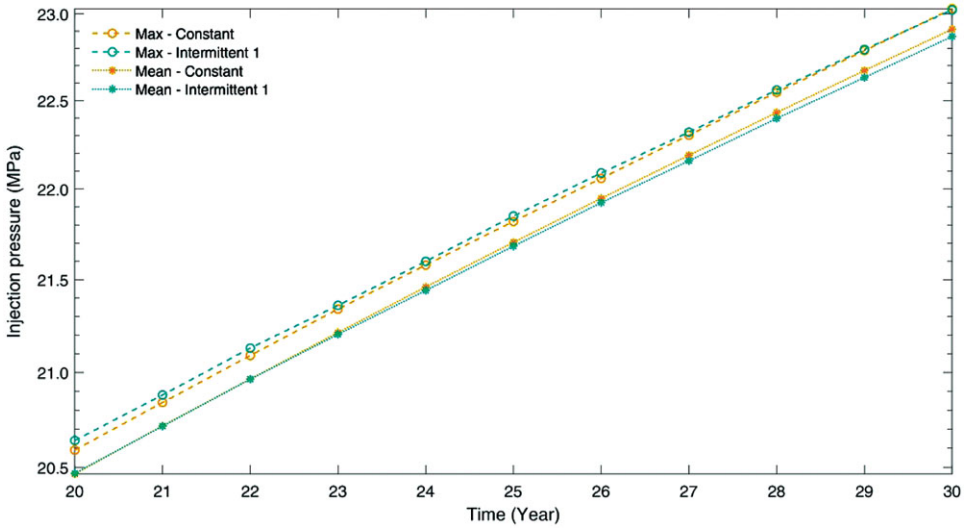

Figure 11. Comparison of maximum and annual mean injection pressure between the constant injection and Intermittent 1 injection in Set 3.

injection scenario has the highest injection pressure exceeding the assumed fracture pressure across the reservoir settings, the intermittent-injection scenario 3 is at risk in Sets 4–7, like that in the base set.

It is only in Set 3 that the highest injection pressure for an intermittent injection (Intermittent 1) is slightly lower than that for the constant injection. This indicates that the annual mean injection pressure in that year for this intermittent injection may be lower than that for the constant injection. In fact, it was found that scenario Intermittent 1 in Set 3 has slightly lower annual mean injection pressure after 22 years compared to results from the constant injection (Fig. 11). It seems that almost all the intermittent injections are not effective in controlling the pressure buildup for the reservoirs considered in this study, only scenario Intermittent 1 in Set 3 showing the potential to control pressure buildup. Given that permeability around the well in Set 3 is nearly double the permeability in the base set, intermittent injection may only be effective to manage pressure buildup for a reservoir with extremely high permeability.

Figure 12 shows the annual mean injectivities of Year 1 and Year 30, as well as the average annual injectivity

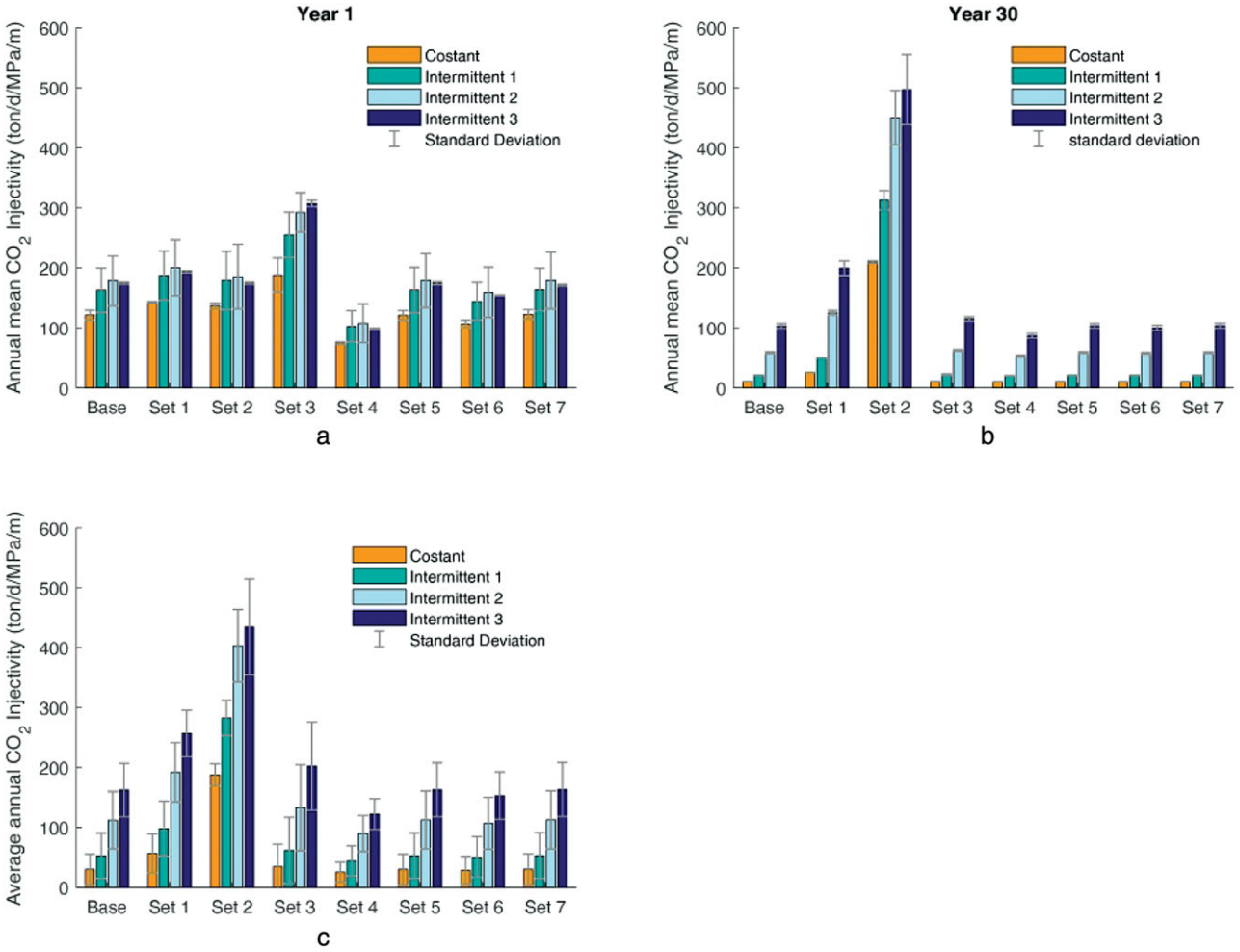

Figure 12. The annual mean injectivity of (a) Year 1 (b) Year 30, as well as (c) average annual injectivity over 30 years for the injection scenarios across the different reservoir settings.

of 30 years for the injection scenarios across the reservoir settings. In Year 1, there are no big differences in the annual mean injectivity for the scenarios between Sets 1, 2, 5–7 and the base set, but Sets 3 and 4 have prominently higher and lower annual mean injectivity for the scenarios than the base set, respectively. This is due to the much different permeability in Sets 3 and 4 around the injector than the base set (Fig. 3), while other sets have similar permeability to the base set. This indicates that the first-year annual mean injectivity is largely influenced by the permeability around the injector. In Year 30, similarity in the annual mean injectivity is observed between Sets 3–7 and the base set, but Sets 1 and 2 have conspicuously higher annual mean injectivity than the base set. This indicates that annual mean injectivity variation is highly sensitive to reservoir compressibility and boundary conditions at long times. Furthermore, the average annual injectivity for an intermittent injection across the different reservoir settings is consistently much higher than that for the constant injection for the same reservoir settings, indicating that the capability of intermittent injections to keep a desired injectivity is persistent across the different sets considered.

In Fig. 13, the number of years of the annual mean injectivity above a reference value increases linearly with the length of injection break, in all of the sets except for Set 2. In Set 2, all injection scenarios exhibit a consistent increase in injectivity with time, with no decline over the 30 years, hence indicating the importance of boundary conditions in determining this relationship. The intermittent injections in Set 3 have a higher first-year injectivity (Fig. 12(-a)) but

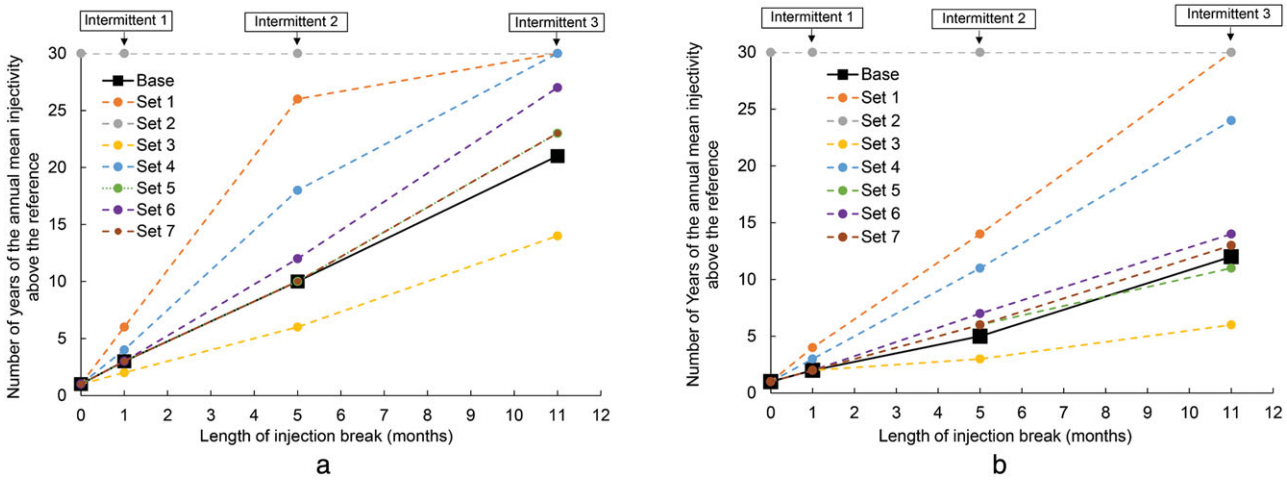

Figure 13. Number of years of the annual mean injectivity being above (a) the first-year annual mean injectivity of the constant injection and above (b) the first-year annual mean injectivity of intermittent injection itself, as a function of the length of injection break.

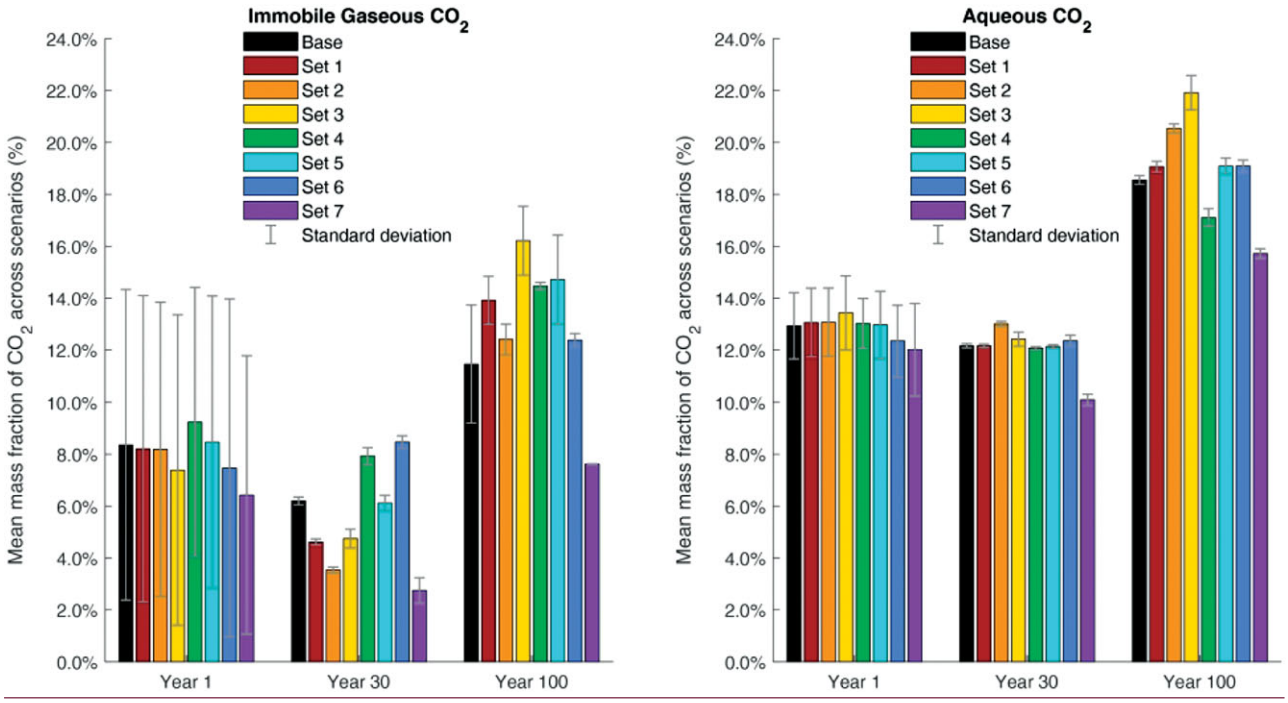

Figure 14. Average mass fractions of immobile gaseous CO_2 and aqueous CO_2 with their standard deviations resulted in by all the injection scenarios in the same reservoir settings at the ends of Year 1, Year 30, and Year 100.

maintain the injectivity above the reference value for a smaller number of years compared to the base set (Fig. 13). The opposite behavior is observed in Set 4. This indicates that, for a reservoir with very high permeability, the intermittent injections may control the pressure buildup, but may not be able to maintain high levels of injectivity for long.

Figure 14 shows the mean mass fractions of immobile gaseous CO_2 and aqueous CO_2 of all injection scenarios in the same reservoir settings at the ends of Year 1, Year 30, and Year 100. Both residual and solubility trapping standard deviations are prominent at the end of the first year but become much smaller at the end of 30 and 100 years. This indicates that the

trapping difference among these scenarios is the most prominent in the first year, but not much for a relatively long time period. The trade-off between residual trapping and CO_2 dissolution trapping at the end of 100 years is observed in some reservoir settings (Sets 4, 5, and 6), but both residual trapping and solubility trapping are found to be high in Sets 1, 2, and 3, and low in Set 7. The reason is not clear. It may relate to the relative permeability models used in simulation. Further research is required to determine the reason why CO_2 dissolution increased with residual trapping in Sets 1, 2, 3, and 7.

Suggestions for future study

Given the assumption of isothermal processes in this study, the effects of strong cooling caused by intermittently injecting supercritical CO_2 into the deep reservoirs have been overlooked. Temperature difference between the injected CO_2 and the reservoir could be several tens of degrees in centigrade. For example, at Cranfield, the reservoir temperature was 125°C, while the CO_2 injection temperature was 35°C.[41,42] The significant cooling may lead to a large thermal stress in the storage formations, which, combined with the injection pressure, may create small thermal fractures in the formation. Once these fractures are created, the permeability around the well would increase by several orders of magnitude, and this would cause a big drop in injection pressure and a substantial increase in injectivity. However, cooling-induced thermal effects on injectivity have not been studied much for CO_2 storage.

As the constant injection leads to a consistent decrease in annual mean injectivity over the years, the annual mean injectivity of the first year has been used as a reference against which the injectivity in later years is assessed. Intermittent injections in this study show that the injectivity can be maintained above the reference for several years. The number of years that injectivity is closely related to not only the length of injection break but also reservoir compressibility, reservoir permeability distributions, and the type of reservoir boundary conditions. These reservoir factors significantly influence the dynamical variations of injectivity over years. The higher the reservoir compressibility, the more years over which intermittent injections maintain the injectivity. Lateral boundary with a constant pressure can totally change the injectivity trend, so a modeler should be very cautious in applying this type of boundary condition. Although a no-flow boundary condition may not be realistic, it is conservative with respect to pressure rise.

According to Law and Bachu,[30] reservoir permeability and relative permeability of CO_2 in brine are two important parameters in determining injectivity. This was confirmed in our study. We found that small changes in the spatial distribution of reservoir permeability could result in larger variations in injectivity, even when the overall average reservoir permeability is kept the same. About relative permeability, although we reduced the residual gas saturation by 40% and adopted a smaller van Genuchten number (m) for liquid to make water movement more sensitive to the saturation change, the results show that these changes only have a significant influence on the injectivity for the first year. Furthermore, the relative permeability and capillary models used in this model are insufficient to illustrate the effects of formations with different pore size distributions on the reservoir responses. So, this aspect also needs further research.

Conclusions

We simulated CO_2 injection into a highly permeable saline aquifer, comparing the effects of different scenarios of injection, with different degrees of interruption within each year (from 0 to 11 months), all aiming to reach the target CO_2 amount. Four criteria were assessed, namely, injection pressure, pressure buildup, injectivity, and trapping efficiency. Our study suggests that while intermittent injection is likely to increase injectivity, it also requires higher injection pressure compared to scenarios where no interruption of injection is involved. Only one intermittent-injection scenario showed the potential to have a lower injection pressure compared to a constant-injection scenario. In addition, the intermittent-injection scenario with the longest break may exceed fracture pressure and therefore incur risks.

There was a consistent and rather rapid decline in injectivity over the years in the constant injection, while the intermittent injections showed a capability to keep the injectivity above a reference value for some years. The number of years for an intermittent injection to keep the injectivity above the reference linearly increases with the length of injection break. Furthermore, injectivity of an intermittent injection was found to peak in a few years after the injection

started. This information can be helpful in optimizing the injection plan, especially if the best use of a reservoir needs to be made in a relatively short period under pressure restrictions. Permeability around the injector largely determines the injectivity for the first year, while reservoir compressibility and type of the boundary conditions are more influential on the injectivity variations with time. Our paper has demonstrated that, for useful predictions to be obtained, accurate estimates of permeability distribution, compressibility, and boundary conditions of the reservoir are critical.

The trapping efficiency may be improved by up to over 15% under intermittent injections, but only in the first few years. In the long term, the differences in trapping efficiencies between the intermittent injections and the constant injection are within 1–3%.

Acknowledgements

This research was supported by the Australian Research Council through Discovery Projects (DP170102886).

The authors also acknowledge the Sydney Informatics Hub and the University of Sydney's high performance computing cluster Artemis for providing the high-performance computing resources that have contributed to the research results reported within this paper.

The authors are also grateful to the two anonymous reviewers for their discerning comments and suggestions on the original manuscript.

References

1. Jean-Baptiste P and Ducroux R, The role of CO_2 capture and sequestration in mitigation of climate change. *CR Geosci* **335**(6–7):611–625 (2003).
2. Lokhorst A and Wildenborg I, Introduction on CO_2 geological storage. Classification of storage options. *Oil & Gas Science and Technology* **60**(3):513–515 (2005).
3. Benson SM and Surles T, Carbon dioxide capture and storage: an overview with emphasis on capture and storage in deep geological formations. *Proc IEEE* **94**(10):1795–1805 (2006).
4. White CM, Strazisar BR, Granite EJ, Hoffman JS and Pennline HW, Separation and capture of CO_2 from large stationary sources and sequestration in geological formations – coalbeds and deep saline aquifers. *J Air Waste Manage* **53**(6):645–715 (2003).
5. IPCC, *IPCC Special Report on Carbon Dioxide Capture and Storage*, ed. by Metz B, Davidson O, de Coninck H, Loos M and Meyer L. Cambridge University Press, Cambridge (2005).
6. Global CCS Institute, *The Global Status of CCS: 2017*. Global CCS Institute, Melbourne (2017).
7. Bachu S, Bonijoly D, Bradshaw J, Burruss R, Holloway S, Christensen NP *et al.*, CO(2) storage capacity estimation: methodology and gaps. *Int J Greenhouse Gas Control* **1**(4):430–443 (2007).
8. USGS, *National Assessment of Geologic Carbon Dioxide Storage Resources – results*. United States Geological Survey (2013).
9. USDOE, *Carbon Sequestration Atlas of United States and Canada*, 1st ed. U.S. Department of Energy (2007).
10. Bradshaw J, Bachu S, Bonijoly D, Burruss R, Holloway S, Christensen NP *et al.*, CO_2 storage capacity estimation: Issues and development of standards. *Int J Greenhouse Gas Control* **1**(1):62–68 (2007).
11. Bachu S, Review of CO_2 storage efficiency in deep saline aquifers. *Int J Greenhouse Gas Control* **40**:188–202 (2015).
12. Kolster C, Agada S, Mac Dowell N and Krevor S, The impact of time-varying CO_2 injection rate on large scale storage in the UK Bunter Sandstone. *Int J Greenhouse Gas Control* **68**:77–85 (2018).
13. Court B, Bandilla KW, Celia MA, Buscheck TA, Nordbotten JM, Dobossy M *et al.*, Initial evaluation of advantageous synergies associated with simultaneous brine production and CO_2 geological sequestration. *Int J Greenhouse Gas Control* **8**:90–100 (2012).
14. Fang Q and Li YL, Exhaustive brine production and complete CO_2 storage in Jianghan Basin of China. *Environ Earth Sci* **72**(5):1541–1553 (2014).
15. Cihan A, Birkholzer JT and Bianchi M, Optimal well placement and brine extraction for pressure management during CO_2 sequestration. *Int J Greenhouse Gas Control* **42**:175–187 (2015).
16. Bandilla KW and Celia MA, Active pressure management through brine production for basin-wide deployment of geologic carbon sequestration. *Int J Greenhouse Gas Control* **61**:155–167 (2017).
17. Farhat K and Benson SM, A technical assessment of CO_2 interim storage in deep saline aquifers. *Int J Greenhouse Gas Control* **15**:200–212 (2013).
18. Wiese B, Nimtz M, Klatt M and Kühn M, Sensitivities of injection rates for single well CO_2 injection into saline aquifers. *Chem Erde* **70**:165–172 (2010).
19. Bannach A, Hauer R, Streibel M, Kühn M and Stienstra G, Stable large-scale CO_2 storage in defiance of an energy system based on renewable energy – modelling the impact of varying CO_2 injection rates on reservoir behavior. *Energy Procedia* **76**:573–581 (2015).
20. Le Guenan T and Rohmer J, Corrective measures based on pressure control strategies for CO_2 geological storage in deep aquifers. *Int J Greenhouse Gas Control* **5**(3):571–578 (2011).
21. Ngoc TDT, Doughty C, Lefebvre R and Malo M, Injectivity of carbon dioxide in the St. Lawrence platform, Quebec (Canada): a sensitivity study. *Greenhouse Gases Sci Technol* **3**(6):516–540 (2013).
22. Li C, Zhang K, Guo CB, Xie J, Zhao J, Li X *et al.*, Impacts of relative permeability hysteresis on the reservoir performance in CO_2 storage in the Ordos Basin. *Greenhouse Gases Sci Technol* **7**(2):259–272 (2017).
23. Pruess K, Oldenburg C and Moridis G, *TOUGH2 User's Guide, Version 2.0*, Report No. LBNL-43134. Lawrence Berkeley National Laboratory, Berkeley, CA (1999).

24. Pruess K, *ECO2N: A TOUGH2 Fluid Property Module for Mixtures of Water, NaCl, and CO_2*, Report No. LBNL-57952. Lawrence Berkeley National Laboratory, Berkeley, CA (2005).
25. Doughty C, *User's Guide for Hysteretic Capillary Pressure and Relative Permeability Functions in TOUGH2*, Report No. LBNL-6533E. Lawrence Berkeley National Laboratory, Berkeley, CA (2013).
26. Zhang K, Wu Y-S and Pruess K, *User's Guide for TOUGH2-MP – A Massively Parallel Version of the TOUGH2 Code*, Report No. LBNL-315E. Lawrence Berkeley National Laboratory, Berkeley, CA (2008).
27. van Genuchten MT, A closed-form equation for predicting the hydraulic conductivity of unsaturated soils. *Soil Sci Soc Am J* **44**(5):892–898 (1980).
28. Parker JC and Lenhard RJ, A model for hysteretic constitutive relations governing multiphase flow .1. Saturation-pressure relations. *Water Resour Res* **23**(12):2187–2196 (1987).
29. Lenhard RJ and Parker JC, A model for hysteretic constitutive relations governing multiphase flow .2. Permeability-saturation relations. *Water Resour Res* **23**(12):2197–2206 (1987).
30. Law DHS and Bachu S, Hydrogeological and numerical analysis of CO_2 disposal in deep aquifers in the Alberta sedimentary basin. *Energy Convers Manage* **37**(6):1167–1174 (1996).
31. Eaton BA, Fracture gradient prediction and its application in oilfield operations. *J Petrol Technol* **21**(10):1353–1360 (1969).
32. Crain ERR, *Crain's Petrophysical Handbook*. Available: http://www.spec2000.net/10-closurestress.htm [30 January 2019].
33. Zhang JC and Yin SX, Fracture gradient prediction: an overview and an improved method. *Pet Sci* **14**(4):720–730 (2017).
34. Birkholzer JT, Zhou QL and Tsang CF, Large-scale impact of CO_2 storage in deep saline aquifers: a sensitivity study on pressure response in stratified systems. *Int J Greenhouse Gas Control* **3**(2):181–194 (2009).
35. Fine RA and Millero FJ, Compressibility of water as a function of temperature and pressure. *J Chem Phys* **59**(10):5529–5536 (1973).
36. Doughty C, Modeling geologic storage of carbon dioxide: comparison of non-hysteretic and hysteretic characteristic curves. *Energy Convers Manage* **48**(6):1768–1781 (2007).
37. Land CS, Calculation of imbibition relative permeability for two and three-phase flow from rock properties. *Soc Petrol Eng J* **8**(2) (1968). https://doi.org/10.2118/1942-PA.
38. Krevor SCM, Pini R, Zuo L and Benson SM, Relative permeability and trapping of CO_2 and water in sandstone rocks at reservoir conditions. *Water Resour Res* **48** (2012). https://doi.org/10.1029/2011WR010859.
39. Doughty C, Estimating plume volume for geologic storage of CO_2 in saline aquifers. *Groundwater* **46**(6):810–813 (2008).
40. Myer LR, *Scoping Calculations on Leakage of CO_2 in Geologic Storage*, Report No. LBNL-59332. Lawrence Berkeley National Laboratory, Berkeley, CA (2007).
41. Lu J, Kordi M, Hovorka SD, Meckel TA and Christopher CA, Reservoir characterization and complications for trapping mechanisms at Cranfield CO_2 injection site. *Int J Greenhouse Gas Control* **18**:361–374 (2013).
42. Gyore D, Stuart FM, Gilfillan SMV and Waldron S, Tracing injected CO_2 in the Cranfield enhanced oil recovery field (MS, USA) using He, Ne and Ar isotopes. *Int J Greenhouse Gas Control* **42**:554–561 (2015).

Cai Li

Cai Li is a postdoctoral researcher at the University of Sydney. She received her PhD in Civil Engineering from The University of Sydney in 2016. Her research focuses on modeling of multiphase flow in porous media including CO_2 storage and compressed air energy storage in aquifers.

Federico Maggi

Federico Maggi is an associate professor in Environmental Engineering and Head of the Environmental Laboratory at The University of Sydney. He is also guest faculty affiliate with the EES at Lawrence Berkeley National Laboratory, CA, USA. He holds a PhD from TUDelft and an ME from Polytechnic University of Torino. His research focuses on environmental modeling of geophysical flows of water, dispersion of chemicals, and biophysical processes.

Keni Zhang

Keni Zhang is a professor at the Institute of Groundwater and Earth Sciences, Jinan University, Guangzhou, China. He also holds a limited appointment at Earth Sciences Division, Lawrence Berkeley National Laboratory, CA, USA. His research focuses on numerical modeling studies and developing parallel computing codes for large-scale, multicomponent, multiphase fluid and heat flow simulations in porous and fractured media. He received his PhD in Groundwater Hydrology from University of Manitoba, Canada.

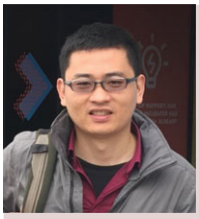

Chaobin Guo

Chaobin Guo works at the Chinese Academy of Geological Sciences as an assistant research fellow after he received his PhD in Thermal Engineering from Tongji University in 2017. His research focuses on the multiphase flow simulation in the terms of aquifer compressed air energy storage, carbon dioxide storage, and underground space utilization.

Yixiang Gan

Yixiang Gan received the Dr-Ing degree (with *summa cum laude*) in Mechanical Engineering from the University of Karlsruhe, Germany. He is a senior lecturer at the School of Civil Engineering at the University of Sydney in Australia and is working on mechanics of heterogenous media, multiphysics, and interface problems.

Abbas El-Zein

Abbas El-Zein is a professor of environmental engineering at the University of Sydney in Australia. He runs the GeoEnvironmental Laboratory at the School of Civil Engineering and is working on the problems in unsaturated soil hydrology and soil mechanics, groundwater contamination, computational modeling, and environmental risk.

Zhejun Pan

Zhejun Pan received his PhD in Chemical Engineering from the Oklahoma State University in Stillwater, Oklahoma in 2004. He is a senior principal research scientist at CSIRO Energy Business Unit. His research interests include gas transport in porous media, gas production from unconventional reservoirs, and CO_2 storage to enhance gas production.

Luming Shen

Luming Shen received his PhD in Civil Engineering from the University of Missouri in Columbia, MO, in 2004. He is an associate professor in the School of Civil Engineering at the University of Sydney in Australia. His research interests include multiscale modeling and simulation, mechanical characterization, fluid–solid interaction, and multiphase flow.

